

Document downloaded from:

<http://hdl.handle.net/10251/117814>

This paper must be cited as:

Teruel, AH.; Pérez-Esteve, É.; Gonzalez-Alvarez, I.; Gonzalez -Alvarez, M.; Costero, AM.; Ferri, D.; Parra Álvarez, M.... (2018). Smart gated magnetic silica mesoporous particles for targeted colon drug delivery: New approaches for inflammatory bowel diseases treatment. *Journal of Controlled Release*. 281:58-69. <https://doi.org/10.1016/j.jconrel.2018.05.007>



The final publication is available at

<https://doi.org/10.1016/j.jconrel.2018.05.007>

Copyright Elsevier

Additional Information

SMART GATED MAGNETIC SILICA MESOPOROUS PARTICLES FOR TARGETED COLON DRUG DELIVERY: NEW APPROACHES FOR INFLAMMATORY BOWEL DISEASES TREATMENT

Adrián H. Teruel,^{a,b} Édgar Pérez-Esteve,^a Isabel González-Álvarez,^c Marta González-Álvarez,^c Ana M. Costero,^{a,b,d} Daniel Ferri,^{a,d} Margarita Parra,^{a,b,d} Pablo Gaviña,^{a,b,d} Virginia Merino,^{a,e} Ramón Martínez-Mañez,^{a,b,f,g,*} and Félix Sancenón^{a,b,f,g}

^a Instituto Interuniversitario de Investigación de Reconocimiento Molecular y Desarrollo Tecnológico (IDM), Universitat Politècnica de València, Universitat de València, Spain.

^b CIBER de Bioingeniería, Biomateriales y Nanomedicina (CIBER-BBN).

^c Departamento de Ingeniería, Sección de Farmacia y Tecnología Farmacéutica, Universidad Miguel Hernandez, 03550, Alicante, Spain.

^d Departamento de Química Orgánica, Universitat de València, Doctor Moliner 50, Burjassot, 46100, Valencia, Spain.

^e Departamento de Farmacia y Tecnología Farmacéutica, Universitat de València 46100, Valencia, Spain.

^f Unidad Mixta de Investigación en Nanomedicina y Sensores. Universitat Politècnica de València, Instituto de Investigación Sanitaria La Fe, Valencia, Spain

^g Unidad Mixta UPV-CIPF de Investigación en Mecanismos de Enfermedades y Nanomedicina, Valencia, Universitat Politècnica de València, Centro de Investigación Príncipe Felipe, Valencia, Spain

ABSTRACT

Magnetic mesoporous silica microparticles were loaded with safranin O (**S1**) and with hydrocortisone (**S2**) and the outer surface functionalized with a bulky azo derivative bearing urea moieties. Aqueous suspensions of both solids at pH 7.4 showed negligible payload release whereas a marked delivery was observed in the presence of sodium dithionite due to the rupture of the azo bonds. Besides, a moderate cargo release was observed at acidic pH due to the hydrolysis of the urea bonds that linked the azo derivative onto the external surface of the inorganic scaffolds. *In vitro* digestion models showed that **S1** and **S2** microparticles could be used for the controlled release of payload in the reducing colon environment (in which azoreductase enzymes are present). On the other hand, *in vivo* pharmacokinetic studies in rats showed that safranin O release from **S1** microparticles was concentrated in colon. The performance of **S2** microparticles for the treatment of colitis in rats (induced by oral administration of a 2,4,6-trinitrobenzenesulfonic acid solution) was tested. The controlled release of hydrocortisone from **S2** in the colon of injured rats induced marked reduction in colon/body weight ratio and in clinical activity score. Also, histological studies showed a marked decrease in inflammation followed by intensive regeneration and almost normal mucosal structure of the individuals treated with **S2**. Besides, the use of a magnetic belt increased the therapeutic performances of **S2** due to an enhanced retention time of the particles in the colon.

KEYWORDS

Colon drug delivery systems; colon targeting; inflammatory bowel disease; mesoporous silica microparticles; gated materials; smart drug delivery

INTRODUCTION

Inflammatory bowel diseases (IBD) are autoimmune, inflammatory, chronic malignances affecting the gastrointestinal tract tissue, mainly the colon, which is a difficult area to treat.[1–5] Although the etiology of IBD is still unknown, some authors have reported that a mix of genetic, environmental factors and some dietetic habits may favor the establishment and proliferation of these diseases. There are two main diseases classified as IBD, ulcerative colitis and Crohn's disease.[3,4] Ulcerative colitis affects exclusively the colon mucosa (first layer from the luminal face) and the injuries caused present a continuous distribution. Meanwhile, Crohn's disease affects all layers (transmural) along the gastrointestinal tract from the mouth until the last portion of the rectus, with injuries distributed in patches (injured areas surrounded by healthy areas). IBD have a big impact in our society since its incidence and prevalence is continuously increasing in both, developed and developing countries.[6–8] Most common treatments for IBD are based on non-specific anti-inflammatory drugs focused on the relief of ulcers and fissures or the damaged tissue.[9–11] These treatments present some disadvantages such as the presence of adverse effects or the low drug efficacy due to the drug systemic absorption in the first segment of the small intestine. Taking this into account, the development of new drug carriers for oral IBD treatment to decrease adverse effects and enhance drug efficacy is a research field with marked interest. With this aim, smart formulations for targeting colon such as pH-responsive biodegradable polymers, time-dependent formulations, pressure responsive systems, osmotic controlled materials, bio-adhesive systems, enzyme triggered prodrugs or drugs coated with enzyme-sensitive polymers have been recently developed.[12–14] In fact, enzymes produced by colon microbiota (such as azoreductase, β -galactosidase, β -xylosidase, nitroreductase, glycosidase deaminase) are ideal candidates to be used as external triggers in the preparation of smart controlled release carriers.[15–17]

From another point of view, the blending of material and supramolecular chemistry concepts has resulted in recent years in the development of innovative examples of smart hybrid organic-inorganic micro or nanodevices able to perform programmed functions.[18] In the vast realm of these smart nanodevices those equipped with "molecular gates" are highly appealing because allow mass transport upon application of an external trigger.[19] These "gated materials" are generally formed by two components: (i) an inorganic porous support, which is able to entrap selected chemicals,

and (ii) supramolecular or (bio)molecular entities, grafted onto the outer surface, which control cargo release upon application of an external stimuli.[20] Dealing with the inorganic supports mesoporous silica has been extensively used for the preparation of these “gated materials”. This is due to its positive features, such as relatively well-known functionalization chemistry, inertness, chemical stability, presence of controlled pore diameter within the nanometric range (ca. 2–3 nm), and large specific surfaces (up to $1200 \text{ m}^2 \text{ g}^{-1}$) and specific volumes.[21] Besides, mesoporous silica can be prepared in the form of nano or microparticles. A high number of gated materials containing different payloads and able to selectively deliver their cargo upon application of chemical, physical or biochemical stimuli have been reported.[19] In fact, the incorporation of gate-like ensembles on the external surface of mesoporous silica particles is a suitable and promising approach to design devices with applications in controlled release protocols in biological, pharmaceutical and medical fields.[22,23] “Gated materials” have mainly been used for drug delivery applications, and the preparation of carriers able to release certain drugs on the site of action at-will, minimizing secondary effects is a benchmark in the treatment of different diseases. Gated mesoporous supports have also been applied recently in sensing/recognition protocols and in chemical communication networks.[24–26] However, it is also apparent from the literature that, gated hybrid organic-inorganic materials have not been used for the development of smart formulations for IBD treatment.

Bearing in mind our interest in the development of silica-based gated materials for controlled release applications,[27–34] we report herein the preparation of micro-sized silica mesoporous solids containing magnetic nanoparticles (**S1** and **S2**) as potential systems designed to release an entrapped cargo in colon. The magnetic character of the solids may be useful to enhance the retention time of the particles in the part of interest of the intestinal tract (ileum or colon). Particles **S1** and **S2**, contained a dye (safranin O) and a model drug (hydrocortisone) in the pores were capped with a bulky azo derivative by means of a urea bond. We demonstrated that the presence of bulky azoderivatives onto the external surface of **S1** and **S2** inhibited cargo delivery yet both solids were able to deliver their cargo in the presence of a reducing agent (sodium dithionite) and to some extent at acidic pH (due to partial hydrolysis of urea bonds that linked the azo derivative onto the inorganic support). Studies on cargo delivery from **S1** in a simulated digestive process in mouth, stomach, small intestine and colon is also reported. Finally,

in vivo studies with **S1** were also performed to check the pharmacokinetics of this new nanodevice and **S2** was used to prove its efficacy in an *in vivo* ulcerative colitis model.

MATERIALS AND METHODS

Chemicals

The chemicals tetraethylorthosilicate (TEOS), *n*-cetyltrimethylammonium bromide (CTABr), sodium hydroxide, triethanolamine (TEAH₃), (3-Isocyanatopropyl)triethoxysilane, iron(III) chloride hexahydrate, iron(II) chloride tetrahydrate, oleic acid, safranin O, triethylamine, Congo red, sodium dithionite, hydrocortisone, and 2,4,6-trinitrobenzenesulfonic acid solution (TNBS), were provided by Sigma-Aldrich. Disodium hydrogen phosphate, sodium dihydrogen phosphate, potassium dihydrogen phosphate, sodium chloride, potassium chloride, sodium acetate anhydrous and all the analytical-grade solvents were purchased from Scharlab. Isoflurane, pentobarbital (dolethal[®]) was acquired from the animal facilities. All products were used as received.

Synthesis of oleic acid-coated magnetic nanoparticles (MNPs)

MNPs were prepared using a modified co-precipitation method. In a typical procedure, FeCl₃·6H₂O (24.0 g, 0.089 mol) and FeCl₂·4H₂O (9.8 g, 0.049 mol) were dissolved in deionized water (100 mL) under nitrogen atmosphere with vigorous stirring at 80°C. Then ammonium hydroxide (50 mL) was added quickly into the solution. The color of the solution immediately turned black and then oleic acid (3.8 g, 0.013 mol) was added after 30 min. The reaction was kept at 80°C for 1.5 h. The final oleic acid-coated MNPs were washed with deionized water until neutral pH. Afterward, the MNPs were transferred into a chloroform solution (30 mg MNPs/mL CHCl₃).

Synthesis of mesoporous silica microparticles containing MNPs (S0)

A chloroform suspension of MNPs (6 mL, 30 mg MNPs/mL CHCl₃) was mixed with an aqueous solution of CTABr (8 mL, 10 mg/mL) and the resulting mixture was homogenized (using a sonicator) and heated. Finally, the suspension was sonicated again and passed through nylon filters (0.45 μM) to ensure MNPs homogeneity.

Magnetic micro-sized MCM-41 particles were synthesized following the so-called “atrane route”. For this purpose, a solution of TEAH3 (25.79 g, 0.173 mol) and NaOH (2 mL of a 6 M solution) was heated to 120°C and then cooled down to 70°C, at this moment TEOS (11 mL, 0.045 mol) was added and the crude reaction was heated up to 120°C. The crude reaction was left cooling down again and CTABr (4.68 g, 0.013 mol) was added at 118°C. Next, water containing MNPs (74 mL of distilled water + 6 mL of the MNPs CTABr-water suspension) was slowly added with vigorous stirring at 70°C. Besides, NaOH (10 mL of a 0.1 M solution) was added to obtain a pH \approx 10.9. After a few minutes, a brownish suspension was formed. This mixture was aged in an autoclave at 100°C for 24 h. The resulting powder was collected by filtration and washed with water. Finally, the solid was dried at 70°C. To prepare the final solid (**S0**), the as-synthesized microparticles were calcined at 550°C using oxidant atmosphere for 5 h in order to remove the template.

Synthesis of 1

Congo red (**1a** in Scheme 2, 8.1 g, 10 mmol) was dissolved in anhydrous *N,N*-dimethylformamide (120 mL) and then (3-Isocyanatopropyl)triethoxysilane (**1b** in Scheme 2, 5.21 mL, 20 mmol) and trimethylamine (2 droplets) were added under argon atmosphere. The crude reaction was allowed to react for 36 h at 100°C. The solvent was eliminated in a rotary evaporator and the final product **1** isolated as dark red oil (11.4 gr, 10 mmol, 96% yield). ¹H NMR (400 MHz, DMSO-D₆): δ =8.79 (d, 2H), 8.47 (d, 2H), 8.36 (s, 2H), 8.12 (d, 4H), 7.96 (d, 4H), 7.78 (br s, 2H), 7.61 (t, 2H), 7.51 (t, 2H), 5.83 (br s, 2H), 3.73 (q, 12H), 2.93 (m, 4H), 1.40 (m, 4H), 1.14 (t, 18H), 0.51 (t, 4H) ppm; ¹³C: δ = 158.3, 152.4, 145.9, 140.1, 132.4, 131.9, 129.1, 128.3, 127.5, 125.0, 124.4, 123.9, 122.9, 118.3, 57.8, 56.2, 42.2, 23.8, 18.5, 18.2, 7.4 ppm. HRMS-EI *m/z*: calcd for C₅₂H₆₄N₈O₁₄S₂Si₂ 572.1766; found: 544.3443 (M–2 EtOH from the trialkoxysilane group).

Synthesis of S1

MCM-41 magnetic mesoporous silica microparticles (**S0**, 160 mg) were suspended in an acetonitrile solution (10 mL) of safranin O (45 mg, 0.8 mmol/g **S0**) under argon atmosphere. The obtained suspension was then stirred at room temperature overnight. Afterward, **1** (1.89 g, 10 mmol/g **S0**) was dissolved in anhydrous *N,N*-dimethylformamide (25 mL) and was added to the microparticle/dye suspension. The

mixture was stirred at room temperature for 6 h in an argon atmosphere. **S1** was isolated as a dark red solid, after several DMF and H₂O washes, by centrifugation and was dried at 40 °C for >24 h.

Synthesis of S2

MCM-41 magnetic mesoporous silica microparticles (**S0**, 330 mg) were impregnated with 3.34 mL of a hydrocortisone ethanolic solution (15 mg/mL) in a 2 cycles impregnation procedure. At this respect, 330 mg of **S0** were sunk in 1.67 mL of hydrocortisone ethanolic solution. Then the particles were left drying at 40°C for 30 min (this step was performed two-times). Afterward, **1** (3.9 g, 10 mmol/g **S0**) was dissolved in a DMF-water 95:5 v/v solution (50 mL) and was added to the loaded microparticles. The mixture was stirred at room temperature for 6 h. **S2** was isolated as a red solid, after several ethanol and H₂O washes, by centrifugation and was dried at 60 °C overnight.

Characterization

Transmission electron microscopy (TEM), scanning transmission electron microscopy (STEM), powder X-ray diffraction (PXRD), thermogravimetric analysis (TGA), N₂ adsorption-desorption, nuclear magnetic resonance (NMR), Fourier transform infrared spectroscopy (FT-IR) and high-performance liquid chromatography (HPLC) techniques were employed to characterize the synthesized materials. TEM and STEM images were acquired using a JEOL JEM-1010 and a JEOL JEM 2100F microscopes, respectively. PXRD measurements were performed on a Bruker D8 Advance diffractometer using CuK α radiation. TGA were carried out on a TGA/SDTA 851e Mettler Toledo balance, using an oxidant atmosphere (air, 80 mL/ min) with a heating program consisting on a heating ramp of 10°C per minute from 393 to 1273 K and an isothermal heating step at this temperature for 30 min. N₂ adsorption-desorption isotherms were recorded with a Micromeritics ASAP 2010 automated sorption analyzer. The samples were degassed at 120°C under vacuum overnight. The specific surface areas were calculated from the adsorption data in the low pressure range using the Brunauer–Emmett–Teller (BET) model. Pore size was determined following the Barrett-Joyner-Halenda (BJH) method. ¹H NMR spectra were recorded using a Bruker AV400 spectrometer. Infrared spectra were recorded using a Bruker Tensor 27 equipment. The HPLC instrument consisted of a Hitachi LaChrom Elite liquid chromatograph (Hitachi Ltd., Tokyo, Japan) equipped

with an auto-sampler (module L-2200), UV detector (model L-2400) and a Kromaphase 100 C18 (150 mm × 4.6 mm i.d., 5- μ m particle size analytical column) (Scharlab, Barcelona, Spain) was used for separations.

Release studies

Controlled release studies from **S1** and **S2** were performed at different pH values (i.e. 2.0, 4.5 and 7.4) and in the presence of a reductive environment (sodium dithionite, which is known to reduce azo linkages). In a typical experiment, 2 mg of the corresponding solid were suspended in water at the selected pH (2 mL) and aliquots were extracted at given times (0, 5 min, 20 min, 40 min, 1 h, 2 h, 4 h, 6 h, 8 h, and 24 h) and centrifuged to remove the solid before analyzing. Controlled release experiments were done in triplicate in order to obtain standard deviation values.

Controlled release from **S1** and **S2** microparticles was also tested under *in vitro* digestion conditions using simulated solutions for saliva, gastric juice, duodenal juice and bile. *In vitro* digestion experiments were carried out with **S1** and **S2** (2 mg) at 37°C (temperature of the human body) and stirring at 100 rpm (in order to ensure the correct suspension of the microparticles). Digestions started by adding simulated saliva fluid (320 μ L) and incubating for 5 min. Then, simulated gastric juice (630 μ L) was added, and the mixture was stirred for 2 h. Later, simulated duodenal juice (630 μ L), bile (320 μ L) and a bicarbonate solution (1 M, 100 μ L) were added simultaneously and the mixture was stirred for another 2 h. Finally, colon fluid was simulated by adding sodium dithionite (2 mg/mL). Aliquots were taken at given times from the beginning of the assay (0, 5, 20, 35, 65, 95, 125, 155, 185, 215, 245, 260 275, 305, 365, 425, 485, 1320 and 1685 min), centrifuged and then analyzed.

To quantify the amount of cargo released **S1** supernatants were loaded into 96 well plate to measure safranin O fluorescence at 571 nm (excitation at 520 nm). For **S2** samples, supernatants were analyzed by HPLC to measure the hydrocortisone released. Calibration curves were used to assess the amounts of safranin O and hydrocortisone released from solids **S1** and **S2** in the different environments tested.

Hydrocortisone quantification

Hydrocortisone was determined by reversed-phase HPLC according to the method described by Navarro and co-workers with several modifications.[35] The HPLC instrument consisted of a Hitachi LaChrom Elite liquid chromatograph (Hitachi Ltd., Tokyo, Japan) equipped with an auto-sampler (module L-2200) and UV detector (model L-2400). A Kromaphase 100 C18 (150 mm × 4.6 mm i.d., 5- μ m particle size analytical column) (Scharlab, Barcelona, Spain) was used for separations. The mobile phase consisted of (A) water and (B) acetonitrile. The program was isocratic for 15 min with 70% A and 30% B. The wavelength of the UV detector was set at 245 nm. Hydrocortisone was quantified according to the external standard method (since no matrix effect was observed) using a calibration curve of the peak area against the compound concentration. The applicability of this method was evaluated by performing a recovery study. For this purpose, digestion fluids were fortified with hydrocortisone at five different concentration levels. In all cases, recovery values, which were estimated from measured versus added amounts of hydrocortisone, were close to 100%. Thus, the results obtained demonstrated the applicability of the proposed methodology for the accurate determination of hydrocortisone in the different fluid samples.

In vivo pharmacokinetic studies

Male Wistar rats were used in accordance with 2010/63/EU directive of 22 September 2010 regarding the protection of animals used for scientific experimentation. The Ethics Committee for Animal Experimentation of the University approved the experimental protocols (Spain, code A1330354541263). Male Wistar rats weighing 300 ± 30 g were anesthetized as described in *in situ* perfusion to allow cannula implantation 24 h before the experiment. A previously described jugular vein permanent cannulation method was used.[36] The implanted cannula allows blood sampling. The animals were randomly assigned ($n = 10$ to 12) to the following groups: Group 1: A volume of 1 mL of safranin O solution (150 μ g/mL saline) was given orally. Group 2: A volume of 1.75 mL of a suspension containing 60 mg of **S1** (that should release ca. 150 μ g of safranin O) was given orally. Group 3: A volume of 1.75 mL of a suspension containing 60 mg of **S1** (that should release ca. 150 μ g of safranin O) was given orally. In addition, the subjects

in this group wore a magnetic belt in the lower part in the waist to increase the retention time of the microparticles in the last segment of the bowel.

Blood samples (0.6–0.7 mL) were withdrawn with heparinized syringes, and replaced by heparinized saline (10 IU/mL) at established sampling times ($t = 15'$, $30'$, $45'$, 1 h, 2 h, 3 h, 4 h and 5 h). Plasma was immediately separated by centrifugation (10,000 rpm for 10 min) and then frozen at -20°C until analysis. At the end of the 5 h the subjects were sacrificed and the cecum, colon and feces were collected and processed to analyze the presence of safranin O. Cecum, colon and feces were separated, suspended into buffer solution (phosphate, pH 6.8), and then centrifuged. Samples were taken and analyzed by HPLC (Waters Alliance[®] e2695, Milford, MA, USA) with fluorescence detector using 520 and 585 nm as excitation and emission wavelengths (Waters 2486, Milford, MA, USA). As mobile phase acetonitrile:water 30:70 v/v with 1% of trifluoroacetic acid was used. A Novapack C₁₈ (WATERS[®]) cartridge-type column (5 μm , 4 mm x 200 mm) was used. Temperature was set at 25°C , 50 μl of injection volume were used and a flow of 1 mL/min was fixed. The method was previously validated with adequate linearity, precision and accuracy ($R > 0.99$ and coefficient of variation $< 5\%$).

In vivo efficacy studies. Induction of colonic inflammation

The studies reported here adhere to the Principles of Laboratory Animal Care and were approved by the institutional ethics committee of the University of Valencia (Spain) according to RD 1201/2005. These studies were carried out on male Wistar rats aged 8–12 weeks and weighing 275–325 g. Animals were housed in an air-conditioned room at $22 \pm 3^{\circ}\text{C}$, $55 \pm 5\%$ humidity, 12 h light/dark cycles and allowed free access to water and laboratory chow for the duration of the studies. To induce the model of chronic inflammation in the rat colon, the method described by Morris and co-workers was followed with several slight modifications.[37] Briefly, rats were arbitrarily separated into treatment groups, with free access to water and then anaesthetized with isoflurane. A graduated rubber canula was inserted rectally into the colon in such a way that the tip was 8 cm proximal to the anus. Then, 0.6 mL of a solution of TNBS (78 mg/kg body weight) dissolved in 50% ethanol (v/v) was instilled into the lumen of the colon through

the rubber probe (total volume 0.6 mL solution). The induction and development of inflammation was monitored every day during the 10 days that lasted the assays.

Treatment studies design

Rats were divided into 5 groups: Group 1 (positive control group, 3 rats) was administered with saline solution (1.5 mL). Group 2 (8 rats) received a suspension of **S0** microparticles (60 mg in 1.5 mL of saline). Group 3 (8 rats) received a hydrocortisone solution (1.5 mg in 1.5 mL of saline). Group 4 (8 rats) received a suspension of **S2** microparticles (60 mg in 1.5 mL of saline). Group 5 (4 rats) received a suspension of **S2** (60 mg in 1.5 mL of saline) and a magnetic belt was attached to the waist of each rat.

The dose of hydrocortisone that received groups three to five, 5.58 mg/kg/day, was calculated from the dose administered to humans.[38] All administrations were done by means of an oral gavage, once a day for three days in the period of the most intensive inflammation (days 3, 4 and 5 after TNBS administration).

Assessment of colonic injury and inflammation

During the 10 days that lasted the assay animals were monitored and clinical activity score of colitis was calculated. At day 10 (after TNBS administration) the rats were killed with an overdose of anesthesia (dolethal[®]) then the abdomen was opened and the distal colon was removed. The samples of inflamed tissue were excised to measure the ratios of distal colon weight to body weight (colon/body ratio) and later a histological evaluation was carried out.

Clinical activity score system

Colitis activity was quantified with a clinical score assessing weight loss, stool consistency and rectal bleeding.[39,40]

Control	Range	Score
	<1%	0
	1-5%	1
% Weight loss	5-10%	2
	10-20%	3
	>20%	4

Stool consistency	Well-formed pellets	0
	Pasty and semi-formed stools	2
	Liquid stools or absence	4
Bleeding	No blood	0
	Positive finding	2
	Gross bleeding	4

The sum of these scores formed the clinical score that ranges from 0 (healthy) to 12 (maximal activity of colitis). Rats that died or had to be sacrificed before day 10 were given a score of 12.

Determination of colon/body weight ratio

Once the animals were sacrificed, the abdomen was opened and the distal colon was rapidly excised and opened longitudinally along the mesenteric edge. The colon was washed with 0.9% (w/v) saline and placed with the mucosal surface upward over a glass plate and then weighted.[41] The ratio of the 8 cm segment distal colon weight was calculated as an index of colonic tissue edema.

Myeloperoxidase activity

The activated neutrophils into the inflamed tissue has peroxidase enzyme substantially expressed. For this reason, myeloperoxidase activity can be measured as index of inflammation. Myeloperoxidase activity was analyzed according to established method with some modification.[42] Colon tissue in presence of 750 μ L of HTAB buffer (0.5% in 80 mM phosphate buffer pH 5.4) on ice was homogenized and centrifuged (-4°C , 10,000 rpm) during 15 min. Supernatant was taken and incubated at 37°C during 5 min with the mixture: 75 μ L of phosphate buffer pH 7.4, 10 μ L of phosphate buffer pH 5.4 and 0.026% hydrogen peroxide (10 μ L). After that, 20 μ L of TMB 18 mM (dissolved in 8% DMF) were added to the previous mixture and incubated. The reaction was stopped after 10 min by the adding of 15 μ L of H_2SO_4 2N. Myeloperoxidase activity was determined in the supernatant by spectrophotometric measures at 450 nm.

Histological evaluation

Two tissue samples (3 cm distal and proximal samples) were excised from each colon and maintained in paraformaldehyde (4%, v/v) for 24 h and then changed to a paraformaldehyde (0.4%, v/v) medium for microscopic studies. These tissue samples were processed routinely and embedded in paraffin. Longitudinal sections (5 μ m) were stained with hematoxylin and eosin. Microscopic assessment by light microscope was performed blind on coded slices.

Statistical analysis

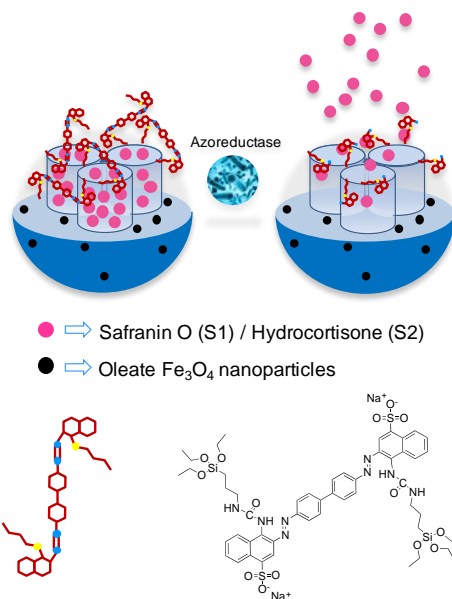
To compare the clinical activity score and the colon/body weight ratio between groups the t-student test was performed using SPSS version 22.0 for Windows (SPSS Inc., USA).

RESULTS AND DISCUSSION

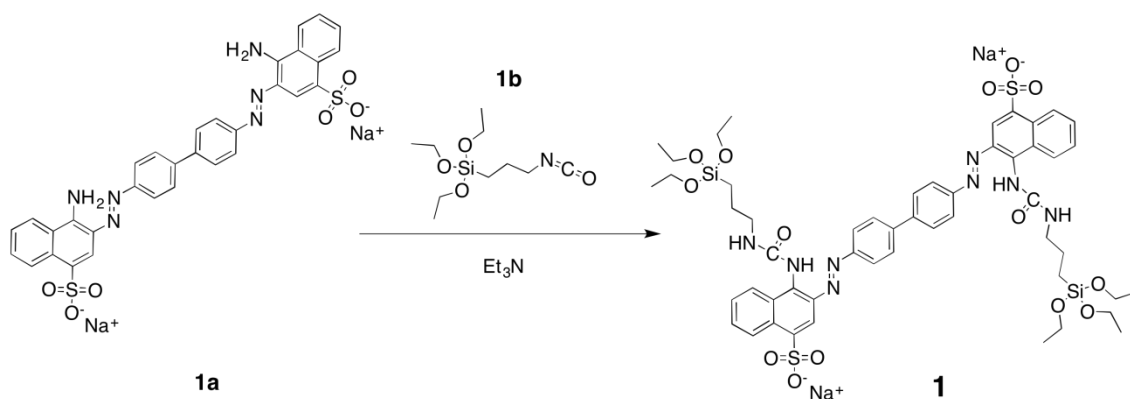
Synthesis of gated magnetic micro-sized mesoporous silica particles

Magnetic nanoparticles (MNPs) coated with oleic acid were prepared by a co-precipitation procedure that used a mixture of FeCl₃ and FeCl₂ and ammonium hydroxide.[43] Moreover, mesoporous silica was prepared following the “atran route” with small modifications.[44,45] In this synthetic protocol *n*-cetyltrimethylammonium bromide (CTABr) was used as structural directing agent and tetraethylortosilicate (TEOS) as silica source. MNPs were suspended in water and incorporated into the synthesis crude before the addition of NaOH. The resulting brownish powder was washed and the surfactant was subsequently removed by calcination. This procedure yielded the final magnetic mesoporous silica micro-sized inorganic solid (**S0**). Once the magnetic mesoporous support was synthesized, the pores of the siliceous phase were loaded with safranin O or hydrocortisone (as a model drug in our study) and the external surface functionalized with the bulky azo derivative **1**. This synthetic protocol yielded micro-sized magnetic solids **S1** and **S2** (see Scheme 1). It was expected that the bulky azo derivative **1** would inhibit the leaching of the cargos from the pores. Moreover, cargo delivery was expected to be observed in the presence of sodium dithionite (able to

broke azo linkages) or partially at acidic pH (due to partial hydrolysis of the urea moiety that linked azo derivative **1** onto the external surface of the inorganic support).



Scheme 1. Magnetic micrometric silica mesoporous support loaded with safranin O (S1) or hydrocortisone (S2) and capped with a bulky azo derivative. Safranin O or hydrocortisone were released in the presence of an azoreductor.



Scheme 2. Synthetic route for the preparation of **1**.

Azo derivative **1** was obtained in a one-step procedure (Scheme 2) reacting Congo red (**1a**) with (3-isocyanatopropyl)triethoxysilane (**1b**). The final azo derivative containing a trilakoxysilane moiety (**1**) was fully characterized using ¹H and ¹³C-NMR and HRMS.

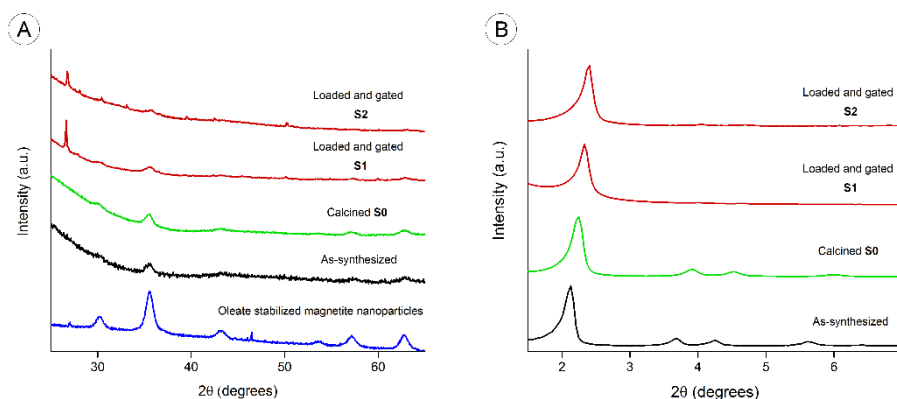


Figure 1. Powder X-ray patterns at A) high angles and B) low angles of oleate-stabilized MNPs, magnetic micrometric mesoporous silica particles as-synthesized, **S0**, **S1** and **S2**.

Characterization of the materials

All the prepared materials were characterized using powder X-ray diffraction (PXRD), transmission electron microscopy (TEM), scanning transmission electron microscopy (STEM), N₂ adsorption-desorption isotherms and thermogravimetric measurements. Figure 1 shows the PXRD patterns (at high and low angles) of oleate-stabilized MNPs, the magnetic mesoporous microparticles as-made, **S0**, **S1** and **S2**. PXRD of oleate-coated MNPs (see Figure 1) showed the five typical high-angle reflections of magnetite phase indexed as (220), (311), (400), (511) and (440) Bragg peaks. The same peaks were observed for the as-made microparticles, **S0**, **S1** and **S2** materials but with a marked decrease in intensity (see again Figure 1). This intensity loss was ascribed to the inclusion of MNPs into the inorganic mesoporous matrix. Low angle PXRD pattern of as-made microparticles (Figure 1) displayed the typical reflections of a hexagonal-ordered mesoporous system that can be indexed as (100), (110), (200) and (210) Bragg peaks. A shift of the (100) peak in calcined **S0** solid was clearly observed. This displacement is consistent with an approximate cell contraction of 3.64 Å and is attributed to the condensation of silanol groups during the calcination step. The presence of the characteristic (100) reflection in the diffraction pattern of **S1** and **S2** clearly indicated that the mesoporous structure was preserved throughout the filling process with safranin O (**S1**) or hydrocortisone (**S2**) and the anchoring of the azo derivative **1** onto the external surface of the microparticles.

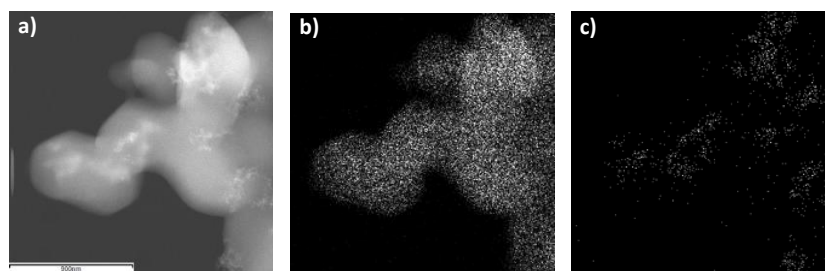


Figure 2. (a) STEM images of **S0** microparticles, (b) silica mapping, and (c) iron mapping.

TEM images of solid **S2** showed the typical porosity associated with MCM-41 mesoporous silica (see Supporting Information). Besides, MNPs were observed, as small dark dots randomly distributed. STEM images of solid **S0** (iron mapping) indicated that MNPs are uniformly distributed through the mesoporous silica microparticles (Figure 2). Moreover, in order to assess the magnetic behavior of **S0**, field dependent magnetization curves measured at 298 K were obtained. The curves displayed no hysteresis loops and showed coercivity values near zero, in agreement with a typical superparamagnetic behavior at room temperature. The saturation magnetization value for **S0** was 1.5 emu/g. This magnetization value is close to those reported in the literature for other magnetic mesoporous silica particles, which are typically in the 1.7-10 emu/g range.[43]

Table 1. BET specific surface area values, pore volumes and pore sizes for **S0**, **S1** and **S2**.

	S_{BET} ($\text{m}^2 \text{g}^{-1}$)	pore volume ^a ($\text{cm}^3 \text{g}^{-1}$)	pore size ^{a,b} (nm)
S0	1097	0.95	2.66
S1	552	0.43	-
S2	355	0.17	-

^a Total pore volume according to the BJH model.

^b Pore size estimated by using the BJH model applied on the adsorption branch of the isotherm, for $P/P_0 < 0.6$, which can be associated to the surfactant generated mesopores.

N₂ adsorption-desorption studies on **S0**, **S1** and **S2** were also carried out (see Supporting Information). Solid **S0** showed a typical curve for mesoporous silica materials, with an adsorption step at intermediate P/P₀ values (0.2-0.4). The isotherm was classified as type IV in which the absorption step deals with nitrogen condensation inside the mesopores. The pore diameter of **S0** was calculated using the Barret-Joyner-Halenda (BJH) method.[46] The narrow BJH pore distribution observed and the absence of a hysteresis loop in the 0.2-0.4 P/P₀ interval suggested the existence of uniform cylindrical mesopores. Values of pore diameter of 2.66 nm and pore volume of 0.95 cm³ g⁻¹, calculated on the adsorption branch of the isotherm, were found. Pore diameter estimated from TEM images agree with this value. The application of the Brunauer–Emmett–Teller (BET) model gave a value of 1097 m² g⁻¹ for the total specific surface area.[47] On the other hand, the N₂ adsorption-desorption isotherms of solids **S1** and **S2** are typical of mesoporous systems with partially filled mesopores, and a significant decrease in both the adsorbed N₂ volume and the specific surface was clearly observed (Table 1). This reduction in the BET surface, compared with that of **S0**, was ascribed to the loading of pores with safranin O (**S1**) or hydrocortisone (**S2**) and the functionalization of the external surface with the bulky azo derivative **1** (for both solids).

Table 2. Content of total organic matter (in g) per gram of SiO₂, content of azo derivative (in g) per gram of SiO₂ and dye/drug released (in µg) per mg of solid in **S1** and **S2**.

solid	organic content (g/g SiO ₂)	gate (g/g SiO ₂)	dye/drug release (µg/mg solid)
S1	0.19	0.13	2.4
S2	0.41	0.15	28.1

Total organic matter on solids **S1** and **S2** was determined by thermogravimetric analysis and ¹H NMR (Table 2). The amount of anchored azo derivative anchored onto **S1** and **S2** was determined by ¹H NMR upon dissolving the corresponding sample in NaOD/D₂O in the presence of tetraethyl ammonium bromide as internal standard.[48] The organic content in solid **S1** was lower than that found in **S2**. This is consistent with

the higher specific surface observed for **S1** (see Table 1) and suggests that loading hydrocortisone into the pores of the inorganic scaffold was more effective than that for safranin O (to obtain **S1**).

FT-IR analysis comparing the calcined framework (**S0**) with the loaded and gated material (**S2**) were carried out to confirm the functionalization of the material (see Supporting Information). **S0** microparticles presented two main bands at 1062 and 954 cm^{-1} that corresponds to Si-O-Si stretching vibrations. Both bands were also present in the FT-IR spectrum of **S2** microparticles. Besides, **S2** also showed signals at 2935 and 2877 cm^{-1} typical of C-H stretching vibrations and attributed to the loaded hydrocortisone and the grafted azo derivative **1**. Moreover, the typical carbonyl (from the urea that linked **1** onto the external surface of the inorganic scaffold) and azo stretching vibrations appeared at 1635 and 1562 cm^{-1} in **S2** microparticles.

Cargo release from **S1** and **S2**

Payload release from solids **S1** and **S2** at acidic (2.0 and 4.5) and neutral (7.4) pH was tested. Besides, the controlled release behavior of both solids at neutral pH (7.4) in the absence or presence of the reducing agent sodium dithionite was also studied.[49,50] These pH values were selected taking into account the possible use of **S2** as vehicle for controlled release in colon and inflammatory bowel disease scenarios. At this respect, pH 2.0 is typical of gastric juices, pH 4.5 is found in the transition from stomach to intestines (this pH can also be found in stomach in fed conditions and in the colon of IBD patients), whereas pH 7.4 is typically found in the intestine. On the other hand, sodium dithionite mimics the presence of azoreductase enzymes on the colon. Cargo release profile for solid **S1** and **S2** are shown in Figures 3 and 4.

As could be seen in Figure 3, aqueous suspensions of **S1** showed negligible safranin O release at neutral pH. However, as a clear contrast, a marked delivery of entrapped safranin O was seen in the presence of sodium dithionite, showing a sustained release profile that reaches ca. 80% of maximum dye delivered after 4 h. The observed delivery is attributed to the sodium dithionite, which is able to reduce azo groups in the capping molecule **1** resulting in pore opening and safranin O release. At pH 4.5, **S1** showed a low dye delivery (ca. 20% of maximum dye released after 8 h). At pH 2.0, safranin O delivery reaches 60% of the maximum drug release after 8 h. The observed release at

acidic pH is attributed to the hydrolysis of urea group in highly acidic environment. Maximum release of safranin O from **S1** was 2.4 $\mu\text{g}/\text{mg}$ solid at pH 7.4 in the presence of a reducing agent. For **S2** solid, a nearly “zero” release of hydrocortisone at pH 7.4 was observed whereas a sustainable delivery of the drug (ca. 75% of maximum hydrocortisone release after 6 h) was produced in the presence of sodium dithionite (see Figure 4). Again, cargo release was ascribed to the reduction of the azo bond by the reducing agent. However, in contrast with the controlled release behavior of **S1** in acidic environments, a “zero” release of hydrocortisone at pH 4.5 and 2.0 was observed. Maximum release of hydrocortisone from **S2** was 28.1 $\mu\text{g}/\text{mg}$ solid at pH 7.4 in the presence of a sodium dithionite. This different behavior is tentatively attributed to the lower solubility of hydrocortisone at acidic pH when compared with safranin O.

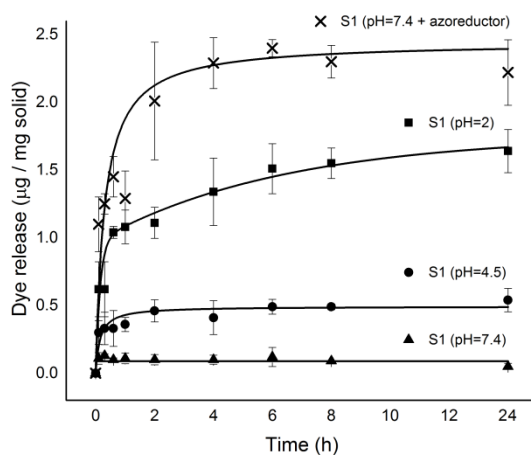


Figure 3. Release kinetics of safranin O from **S1** in aqueous solution at pH \approx 2 (square), pH \approx 4.5 (circle), pH \approx 7.4 (triangle) and pH \approx 7.4 in the presence of sodium dithionite (2 mg/mL) (cross).

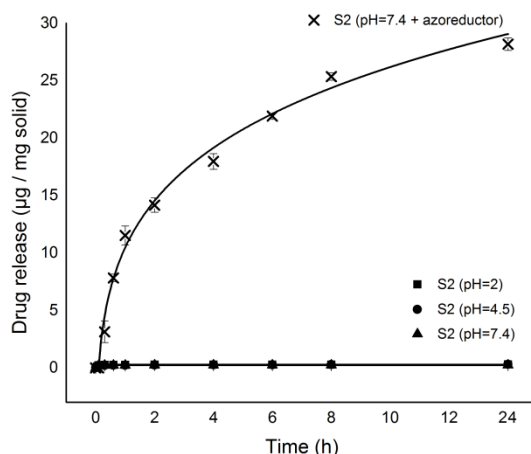


Figure 4. Release kinetics of hydrocortisone from **S2** in aqueous solution at pH \approx 2 (square), pH \approx 4.5 (circle), pH \approx 7.4 (triangle) and pH \approx 7.4 in the presence of sodium dithionite (2 mg/mL) (cross).

In vitro digestion model assay

Despite the partial payload delivery from **S1** at acidic pH shown above, it has to be noted that permanence of the particles in the stomach is usually less than 2 h and therefore only a partial cargo delivery is expected to occur before targeting colonic tissues. In fact, in order to study more in-depth, the possible application of the prepared magnetic microparticles as suitable carriers for cargo delivery in colon, payload release from **S1** was further tested in a model of digestion using simulated solutions. The model used was a modification of the introduced by Oomen and co-workers which is a three-step procedure simulating digestive process in mouth, stomach and small intestine.[51,52] Moreover, we introduced a fourth step to simulate the digestive process in colon. The results obtained with **S1** microparticles are shown in Figure 5.

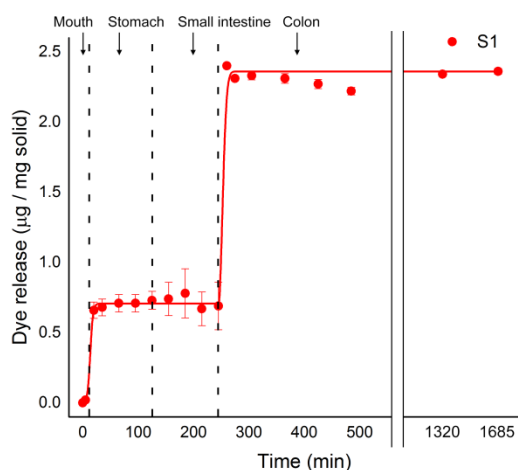


Figure 5. Release kinetics of safranin O from **S1** in simulated GIT fluids.

As could be seen in Figure 5, a nearly “zero release” was observed during the first 5 min in which the solid was in contact with simulated saliva. However, a moderate cargo release (0.6 µg/mg of safranin O for **S1**) was observed in the stomach due to partial pore opening (hydrolysis of the urea bond that linked the bulky azo derivative onto the microparticle surface) in the acidic environment of this part of the GIT. In conditions simulating small intestine, no further delivery of safranin O was observed. Finally, a marked cargo release was found in simulated colon conditions (1.8 µg/mg of safranin O for **S1**). This marked delivery observed is clearly related with the presence of sodium dithionite, which is able to reduce azo bonds of the capping ensemble in **S1** microparticles.

In vivo pharmacokinetics studies

To prove the specific colon delivery and quantify cargo release from the synthesized microparticles in plasma and colon, *in vivo* pharmacokinetic studies were carried out. For this purpose, male Wistar rats were divided into three groups (see Experimental section). Rats in group 1 were treated with 1 mL of safranin O solution (150 µg/mL saline). The subjects from group 2 were treated with 1.75 mL of a suspension of **S1** microparticles (containing 60 mg of solid that releases ca. 150 µg of safranin O). Finally, group 3 rats were subjected to the same treatment than those in group 2 but, in addition, a magnetic belt in the lower part of the waist was implemented in order to increase the retention time of the microparticles in the last segment of the bowel due to

the presence of magnetic nanoparticles in **S1**. Safranin O concentrations in plasma are shown in Figure 6. As could be seen, subjects from group 1 (that received the safranin O solution) showed high plasma levels of the dye (maximum value was ca. 0.35 $\mu\text{g}/\text{mL}$ after 30 min). However, rats in group 2 and 3 presented negligible safranin O systemic absorption. The marked decrease of safranin O in the plasma of the subjects pertaining to groups 2 and 3 indicate a remarkable protection of the cargo in **S1** that inhibited absorption of the cargo in the intestine.

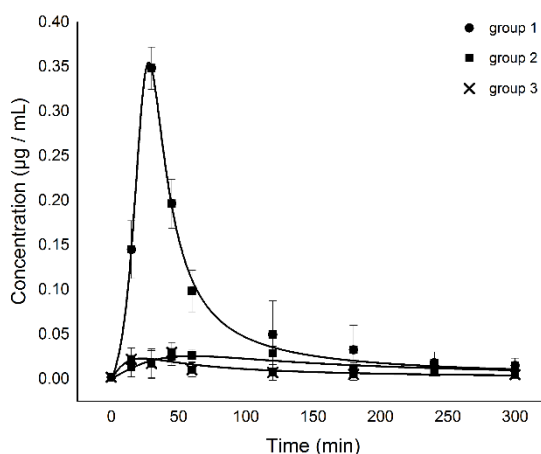


Figure 6. Safranin O concentration ($\mu\text{g}/\text{mL}$) in plasma for subjects of group 1 (safranin O solution), group 2 (**S1** suspension) and group 3 (**S1** suspension + magnetic belt).

Besides, the presence of safranin O in cecum, colon and feces released from the particles was also evaluated. As could be seen in Figure 7, subjects in group 1 showed negligible safranin O levels in cecum, colon and feces. Moreover, the levels of the dye in cecum and feces (for the individuals of groups 2 and 3 treated with **S1**) were lower when compared to levels observed in colon. The remarkable concentration of safranin O in colon for subjects from groups treated with **S1** (2 and 3) strongly suggested that microparticles were opened selectively in the reductive environment of this part of the GIT. Besides, safranin O levels in colon of individuals of group 3 are significantly higher than those found for rats in group 2. This fact was ascribed to the enhanced retention of **S1** microparticles in the colon because of the presence of the magnetic belt.

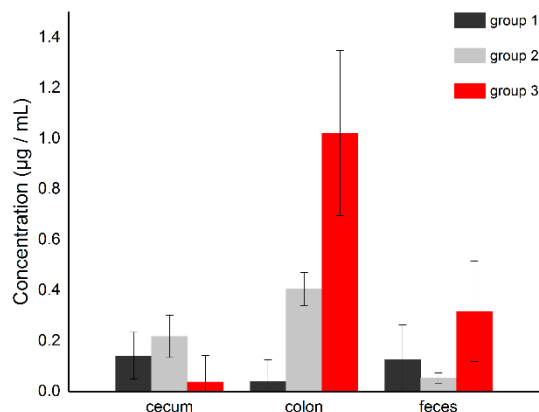


Figure 7. Safranin O concentration ($\mu\text{g}/\text{mL}$) released from the particles in cecum, colon and feces for subjects of group 1 (safranin O solution), group 2 (**S1** suspension) and group 3 (**S1** suspension + magnetic belt).

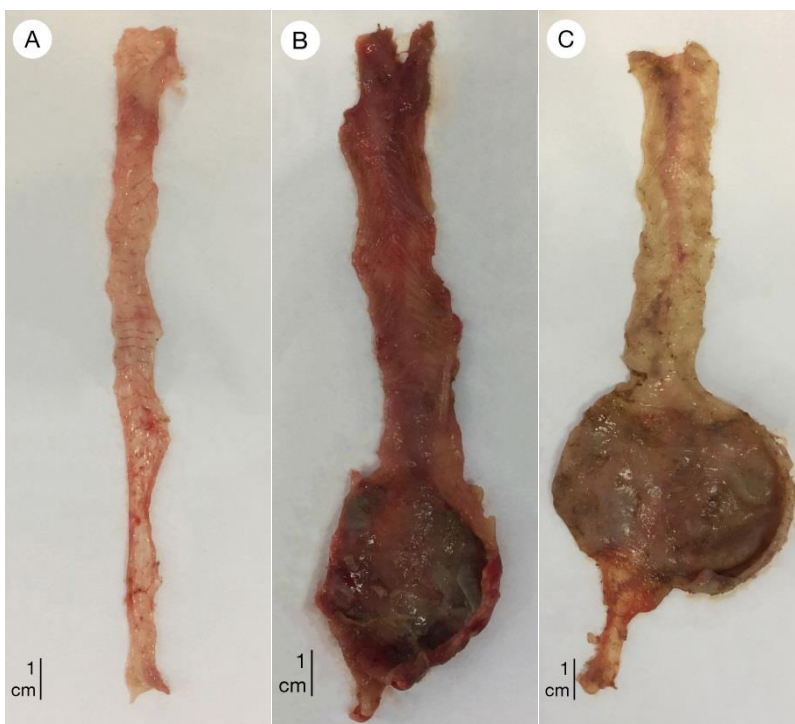
The results presented above evidence the specific safranin O delivery into the colon and the avoidance of systemic absorption when rats were treated with **S1**. Moreover, improved results (in terms of concentration of dye in colon) were obtained for rats wearing a magnetic belt.

In vivo efficacy studies. Induction of colonic inflammation

In order to test the *in vivo* efficacy of the prepared microparticles a model of chronic inflammation in colon was used. For this purpose, male Wistar rats were treated with an enema containing trinitrobenzene sulfonic acid (TNBS) in ethanol-water 1:1 v/v mixture (see Experimental section for details). The main advantages of this model are its simplicity, reproducibility and time and dose related development of inflammation.[53,54] The development of the inflammation was monitored daily. It was observed that rats suffered from diarrhea and weight-loss but not rectal bleeding.

The efficacy of the magnetic microparticles loaded with hydrocortisone (**S2**) for the treatment of TNBS-induced colitis in rats was assessed. For this purpose, rats were divided into five groups (see Experimental section for details). Rats in group 1 were treated with 1.5 mL of saline solution (positive control). Group 2 was formed by rats treated with a suspension (60 mg in 1.5 mL of saline) of **S0** microparticles (as a control

to assess the effect of the inorganic magnetic scaffold). Individuals in group 3 received a hydrocortisone solution (1.5 mg in 1.5 mL of saline). A suspension of **S2** microparticles (60 mg in 1.5 mL of saline) was administered to rats pertaining to group 4. Finally, group 5 was constituted by rats treated with a suspension of **S2** (60 mg in 1.5 mL of saline) wearing also a magnetic belt to evaluate if there was any improvement when the retention time of microparticles at the end of the GIT was lengthened. The efficacy of **S2** microparticles was evaluated by comparing the clinical activity score (see Experimental section), colon/body ratio (in g/g) and histological damage among the different groups.



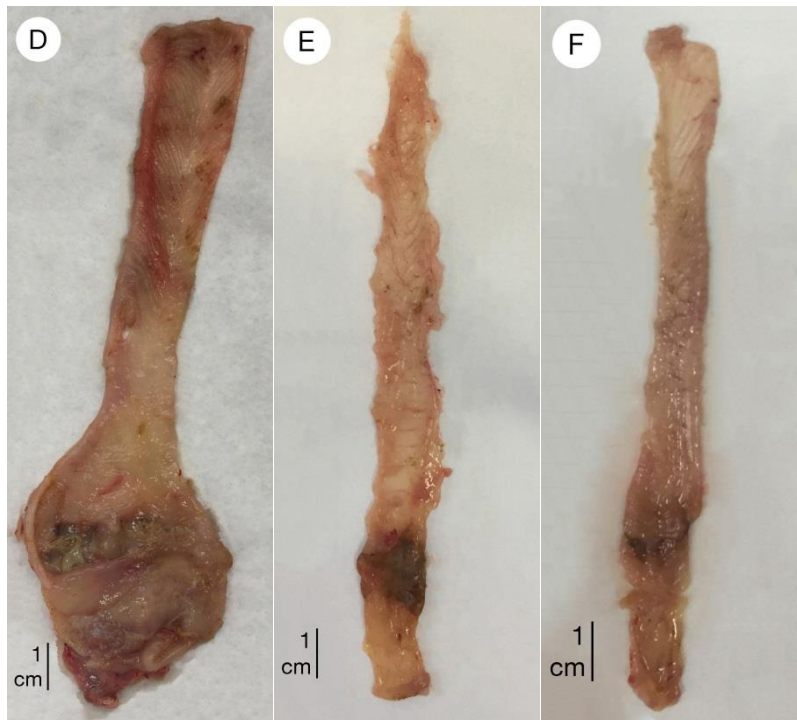


Figure 8. Pictures of rat colon after the induction of colitis with TNBS sacrificed on day 10. A) healthy control (no TNBS administered); B) group 1 as positive control (treated with saline solution); C) group 2 (treated with **S0**); D) group 3 (treated with hydrocortisone); E) group 4 (treated with a **S2** suspension); F) group 5 (treated with **S2** + magnetic belt).

In a first step, the colon appearance of rats pertaining to groups 1-5 was visually assessed (Figure 8). All rats from groups 1 to 5 were killed on day 10. Figure 8A show the typical aspect of a healthy colon in rats not treated with TNBS. Figure 8B and 8C show opened colons of rats pertaining to groups 1 (treated with saline as positive control) and 2 (administered with a suspension of **S0** microparticles). Both colons are closely similar showing necrotic tissue and presented a thick and rigid bowel. When hydrocortisone was administered (rats of group 3, see Figure 8D) some tissues started to heal, necrotic zones and thickened tissues decreased to some extent but they were still largely present. As clear contrast, colon of rats treated with **S2** microparticles (Figure 8E) showed middle to mild injuries with the presence of necrotic areas but with tissues no longer thickened. Finally, Figure 8F showed the open colon of a rat pertaining to group 5 (treatment with **S2** microparticles and the rats wearing a magnetic belt). As could be seen, the aspect of the colon resembles that of healthy individuals (see Figure

8A) presenting small injuries. The observed results pointed to a selective release of the entrapped hydrocortisone in **S2** microparticles in the colon of TNBS-treated rats. Besides, the efficacy of the treatment of **S2** coupled to a magnetic field was higher than that found with the microparticles alone. This fact was ascribed to the enhanced retention time of **S2** microparticles in colon that resulted in a more effective delivery of hydrocortisone in the injured tissues. In fact, after the treatment, rats from group 4 and 5 started to gain weight and have normal stool. Besides, some of the rats from group 3 (receiving hydrocortisone solution) gained weight and improved their health condition as well. On the contrary, rats treated with saline solution or **S0** (groups 1 and 2) continued losing weight and had diarrhea during all the experiment time.

In a second step, the effects of different formulations on the colon/body ratio and clinical activity score were assessed (see Experimental section). The obtained results are shown in Figures 9 and 10. As could be seen in Figure 9, the colon/body ratio in TNBS-treated rats administered with saline (positive control) was in the 0.30-0.33 g/g interval. Nearly the same interval was observed for rats in group 2 (treated with **S0** microparticles). However, as a clear contrast, a marked reduction in the colon/body ratio for rats in groups 4 and 5 was observed (ca. 0.04-0.19 g/g for individuals treated with **S2** and wearing a magnetic belt). These reductions in the colon/body ratio indicated that **S2** microparticles reached the site of action and released hydrocortisone more efficiently. These results contrast with those obtained in group 3 (rats treated with hydrocortisone administered orally as a solution) that presented high variability with cases of real improvements mixed with individuals in which no effect was observed. This was reflected in a large colon/body ratio range (0.05-0.30 g/g) and suggested that hydrocortisone is probably adsorbed before the drug reaches the site of action.

Almost the same results were obtained with the clinical activity score (see Figure 10). Colitis activity was quantified with a clinical score assessing weight loss, stool consistency and rectal bleeding. The sum formed the clinical score that ranges from 0 (healthy) to 12 (maximal activity of colitis).[39,40] Rats that died or had to be sacrificed before day 10 were given a score of 12. As could be seen in Figure 10, rats in group 1 (treated only with saline) presented a clinical score in the 7-9.5 range indicative of marked colitis activity. Besides, a marked reduction of the clinical activity score was observed in the groups treated with **S2** microparticles (4 and 5) indicative of a proper delivery of hydrocortisone in the injured colonic tissue.

Moreover, myeloperoxidase measurements agree with the clinical activity score obtained. These measurements indicated a myeloperoxidase activity decrease of 47% after administration of free hydrocortisone. However, after oral administration of **S2** microparticles in rats, a marked 94% decrease in myeloperoxidase activity was observed. This reduction in enzyme activity clearly indicated that inflammation was reduced with the **S2** administration.

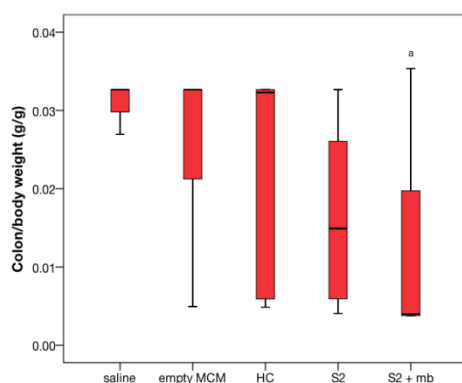


Figure 9. Colon/body weight ratio of animals with TNBS-induced colitis after treatment with saline solution (group 1, positive control), **S0** (group 2), hydrocortisone (group 3), **S2** (group 4) and **S2** + magnetic belt (group 5). In each box is represented the median value, 25% and 75% percentils, minimal and maximal values (^a statistical significant difference ($P < 0.05$) compared to saline).

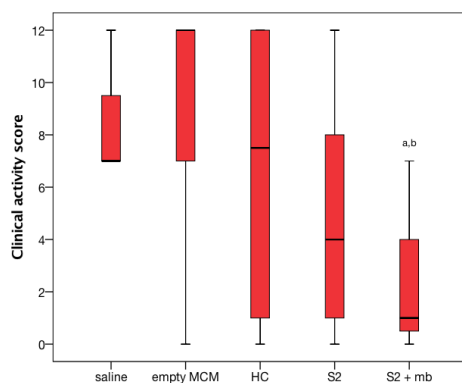
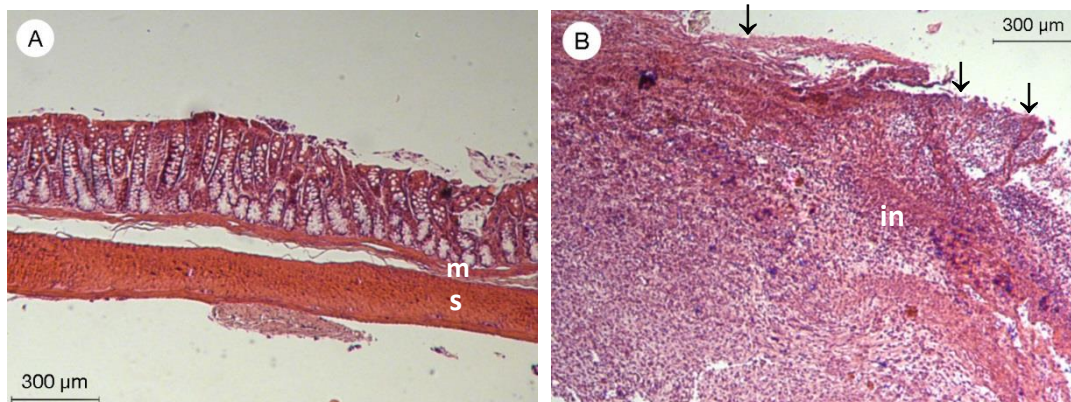


Figure 10. Clinical activity score of animals with TNBS-induced colitis after treatment with saline solution (group 1, positive control), **S0** (group 2), hydrocortisone (group 3) **S2** (group 4) and **S2** + magnetic belt (group 5). In each box is represented the median value, 25% and 75% percentils, minimal and maximal values (^{a,b} statistical significant difference ($P < 0.05$) compared to saline and empty MCM, respectively).

Histological evaluation

Finally, a histological examination of colon tissues of a healthy rat (control without TNBS administration), and of individuals treated with saline (group 1), **S0** (group 2), hydrocortisone (group 3), **S2** (group 4) and **S2** + magnetic belt (group 5) was carried out. All samples were taken from rats sacrificed on the 10th day after administration of TNBS (see Experimental section for details). The obtained results are shown in Figure 11. Rats without TNBS treatment showed a normal colon structure with healthy mucosa, enterocytes and goblet cells and between them connective tissue (lamina propria), muscularis mucosae and normal submucosa and muscularis externa (see Figure 11A). Tissues of individuals of groups 1 and 2 showed loss of the necrotic mucosa and substitution with granulation tissue. A strong inflammatory process was present in the lamina propria, submucosa and muscularis externa (Figures 11B and 11C). As can be seen in Figure 11B and 11C, process of ulceration with fibrinoid necrosis of the mucosal surface and granulation tissue below the necrotic tissue were observed. Animals in group 3 presented superficial erosion, thinning of the mucosa accompanied by thickening of the muscularis mucosae, and a chronic inflammatory process that affects the mucosa and submucosa with early development of lymphoid follicles (see Figure 11D). Besides, few parts with normal mucosa structure but presence of strong follicular hyperplasia in the muscularis externa and parts with necrosis, loss of mucosa and substitution with granulation tissue and inflammation process were also observed (see again Figure 11D). On the other hand, animals that received **S2** microparticles treatment (groups 4 and 5) showed substantially normal mucosal structure with slight presence of chronic inflammation in the muscularis propria (see Figure 11E and 11F).



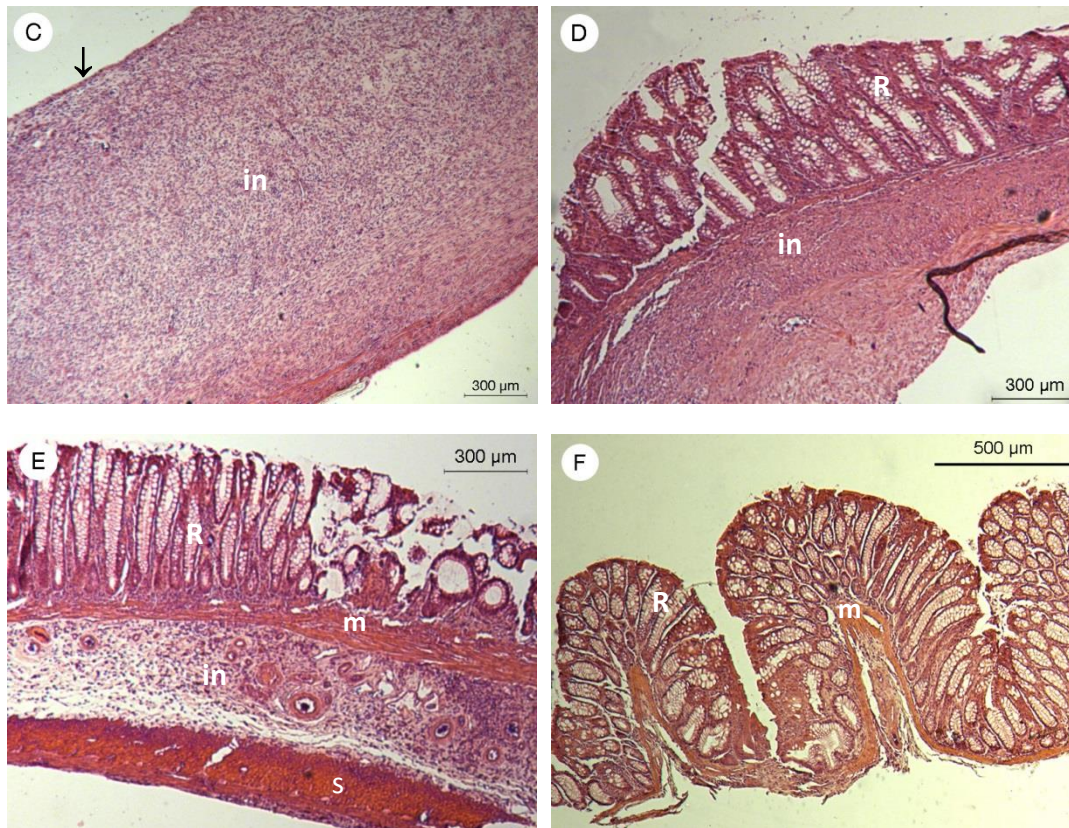


Figure 11. Histology of a representative colon specimen of A) healthy rat; B) group 1 as positive control (treated with saline solution); C) group 2 (treated with **S0**); D) group 3 (rats administered with hydrocortisone); E) group 4 (subjects treated with a **S2** suspension); F) group 5 (treated with **S2** + magnetic belt). m: muscularis mucosae, s: submucosa, in: infiltration, R: regenerated crypts and mucosal architecture, ↓ absence of surface epithelium.

The results of the histological studies showed that tissues of saline treated TNBS individuals (group 1) presented strong inflammation accompanied with necrosis and loss of the mucosa. Similar results were obtained for tissues isolated from individuals of group 2 (treated with suspensions of **S0** microparticles). As marked contrast, tissues from rats in groups 4 and 5 (treated with **S2** and **S2** + magnetic belt respectively) showed a decrease in inflammation followed by intensive regeneration and almost normal mucosal structure.

Histological evaluation provided additional information to that obtained by the clinical activity score and colon/body weight ratio observations, thus confirming the usefulness

of the **S2** microparticles in the treatment of IBD. **S2** were even more effective if a magnetic field was applied to retain particles in the damaged intestinal areas. The results obtained with **S2** microparticles showed enhanced efficacy with respect of other formulations [42,55] with the added benefit of having no systemic intervention.

CONCLUSIONS

A new oral colon drug delivery device was designed, prepared and its efficacy in the treatment of IBD was evaluated *in vivo* in a TNBS colitis induced rat model. The nanodevices consisted on magnetic mesoporous silica microparticles loaded with safranin O (**S1**) or with hydrocortisone (**S2**) and functionalized in the external surface with a bulky azo derivative covalently grafted through urea bonds. Both materials remained capped at neutral pH whereas a marked payload release was observed in the presence of a reducing agent (such as sodium dithionite). This cargo delivery was ascribed to the reduction of azo bonds in the capping ensemble. Besides, a certain safranin O release was observed at acidic pH mainly related with the partial hydrolysis of the urea bonds that linked the azo derivatives onto the external surface of the loaded scaffold. *In vivo* pharmacokinetic studies carried out with **S1**, evidenced specific safranin O delivery in colon and the absence of safranin O systemic absorption (negligible concentrations of safranin O in plasma). Moreover, improved results (in terms of concentration of dye in colon) were obtained for rats wearing a magnetic belt. Colon/body weight ratio, clinical activity score systems and histology evaluation showed that rats with a model of chronic inflammation in colon and treated with **S2** microparticles had an improvement in the pathology, being more effective when a magnetic field was externally applied to lengthen the retention time in the areas of interest. **S2** and specially **S2** + magnetic belt improved efficacy of hydrocortisone in the *in vivo* induced colitis model. In conclusion, we demonstrated that our system can be used to specifically deliver drugs or other agents in the last part of intestine while decreasing the systemic absorption; both effects contribute to increase efficacy for the treatment of inflammatory bowel disease and to reduce adverse effects of drugs.

Acknowledgements

We thank the Spanish Government (projects MAT2015-64139-C4-1-R and AGL2015-70235-C2-2-R (MINECO/FEDER)) and the Generalitat Valenciana (project

PROMETEOII/2014/047) for support. AHT thanks to the Spanish MEC for his FPU grant. The authors also thank the Electron Microscopy Service at the Universitat Politècnica de València for support. SCSIE (Universitat de València) is also gratefully acknowledged for all the equipment employed. NMR was registered at the U26 facility of ICTS “NANBIOSIS” at the Universitat de València. The authors thanks Dr. L. A. Villaescusa for his helpful discussion about the ¹H NMR analysis of the composition of loaded and functionalized supports.

References

- [1] A. Kaser, S. Zeissig, R.S. Blumberg, Inflammatory Bowel Disease, *Annu. Rev. Immunol.* 28 (2010) 573–621.
- [2] X.-M. Xu, H.-J. Zhang, miRNAs as new molecular insights into inflammatory bowel disease: Crucial regulators in autoimmunity and inflammation, *World J. Gastroenterol.* 22 (2016) 2206–2218.
- [3] B.B. Crohn, An historic note on ulcerative colitis, *Gastroenterology.* 42 (1962) 366–367.
- [4] E.M. DeFilippis, R. Longman, M. Harbus, K. Dannenberg, E.J. Scherl, Crohn’s Disease: Evolution, Epigenetics, and the Emerging Role of Microbiome-Targeted Therapies, *Curr. Gastroenterol. Rep.* 18 (2016) 13.
- [5] B.B. Crohn, L. Ginzburg, G.D. Oppenheimer, Regional ileitis: a pathologic and clinical entity. 1932, *Mt. Sinai J. Med.* 67 (2000) 263–268.
- [6] Y. Ye, Z. Pang, W. Chen, S. Ju, C. Zhou, The epidemiology and risk factors of inflammatory bowel disease, *Int. J. Clin. Exp. Med.* 8 (2015) 22529–22542.
- [7] N.A. Molodecky, I.S. Soon, D.M. Rabi, W.A. Ghali, M. Ferris, G. Chernoff, E.I. Benchimol, R. Panaccione, S. Ghosh, H.W. Barkema, G.G. Kaplan, Increasing incidence and prevalence of the inflammatory bowel diseases with time, based on systematic review, *Gastroenterology.* 142 (2012) 46–54.
- [8] A.E. M’Koma, Inflammatory bowel disease: an expanding global health problem, *Clin. Med. Insights. Gastroenterol.* 6 (2013) 33–47.
- [9] M. Fakhoury, R. Negrulj, A. Mooranian, H. Al-Salami, Inflammatory bowel disease: Clinical aspects and treatments, *J. Inflamm. Res.* 7 (2014) 113–120.
- [10] C. Mowat, A. Cole, A. Windsor, T. Ahmad, I. Arnott, R. Driscoll, S. Mitton, T.

- Orchard, M. Rutter, L. Younge, C. Lees, G.-T. Ho, J. Satsangi, S. Bloom, on behalf of the I.S. of the B.S. of IBD Section of the British Society of Gastroenterology, Guidelines for the management of inflammatory bowel disease in adults, *Gut*. 60 (2011) 571–607.
- [11] B. Feagan, J. MacDonald, Oral 5-aminosalicylic acid for induction of remission in ulcerative colitis, *Cochrane Database Syst. Rev.* 17 (2012) CD000543.
- [12] K. Malik, L. Goswami, P. Kothiyal, S. Mukhopadhyay, A Review on Colon Targeting Drug Delivery System: Novel Approaches, Anatomy and Evaluation, *Pharma Innov. J.* 1 (2012) 01–12.
- [13] C. Lautenschläger, C. Schmidt, D. Fischer, A. Stallmach, Drug delivery strategies in the therapy of inflammatory bowel disease, *Adv. Drug Deliv. Rev.* 71 (2014) 58–76.
- [14] S. Hua, E. Marks, J.J. Schneider, S. Keely, Advances in oral nano-delivery systems for colon targeted drug delivery in inflammatory bowel disease: selective targeting to diseased versus healthy tissue, *Nanomedicine*. 11 (2015) 1117–1132.
- [15] V.R. Sinha, R. Kumria, Microbially triggered drug delivery to the colon, *Eur. J. Pharm. Sci.* 18 (2003) 3–18.
- [16] A. Rubinstein, Microbially controlled drug delivery to the colon, *Biopharm. Drug Dispos.* 11 (1990) 465–475.
- [17] V. V. Prasanth, R. Jayaprakash, S.T. Mathew, Colon specific drug delivery systems: A review on various pharmaceutical approaches, *J. Appl. Pharm. Sci.* 2 (2012) 163–169.
- [18] A.B. Descalzo, R. Martínez-Máñez, F. Sancenón, K. Hoffmann, K. Rurack, The supramolecular chemistry of organic-inorganic hybrid materials, *Angew. Chem. Int. Ed.* 45 (2006) 5924–5948.
- [19] E. Aznar, M. Oroval, L. Pascual, J.R. Murguía, R. Martínez-Máñez, F. Sancenón, Gated Materials for On-Command Release of Guest Molecules, *Chem. Rev.* 116 (2016) 561–718.
- [20] C. Giménez, C. de la Torre, M. Gorbe, E. Aznar, F. Sancenón, J.R. Murguía, R. Martínez-Máñez, M.D. Marcos, P. Amorós, Gated mesoporous silica nanoparticles for the controlled delivery of drugs in cancer cells, *Langmuir*. 31 (2015) 3753–3762.
- [21] A. Stein, Advances in microporous and mesoporous solids - Highlights of recent progress, *Adv. Mater.* 15 (2003) 763–775.

- [22] Z. Li, J.C. Barnes, A. Bosoy, J.F. Stoddart, J.I. Zink, Mesoporous silica nanoparticles in biomedical applications, *Chem. Soc. Rev.* 41 (2012) 2590-2605.
- [23] T.L. Doane, C. Burda, The unique role of nanoparticles in nanomedicine: imaging, drug delivery and therapy, *Chem. Soc. Rev.* 41 (2012) 2885-2911.
- [24] F. Sancenón, L. Pascual, M. Oroval, E. Aznar, R. Martínez-Mañez, Gated Silica Mesoporous Materials in Sensing Applications, *ChemistryOpen*. 4 (2015) 418–437.
- [25] C. Giménez, E. Climent, E. Aznar, R. Martínez-Mañez, F. Sancenón, M.D. Marcos, P. Amorós, K. Rurack, Towards chemical communication between gated nanoparticles, *Angew. Chem. Int. Ed.* 53 (2014) 12629–12633.
- [26] A. Llopis-Lorente, P. Díez, A. Sánchez, M.D. Marcos, F. Sancenón, P. Martínez-Ruiz, R. Villalonga, R. Martínez-Mañez, Interactive models of communication at the nanoscale using nanoparticles that talk to one another, *Nat. Commun.* 8 (2017) 15511.
- [27] M. Oroval, P. Díez, E. Aznar, C. Coll, M.D. Marcos, F. Sancenón, R. Villalonga, R. Martínez-Mañez, Self-Regulated Glucose-Sensitive Neoglycoenzyme-Capped Mesoporous Silica Nanoparticles for Insulin Delivery, *Chem. Eur. J.* 23 (2017) 1353–1360.
- [28] A. García-Fernández, G. García-Laínez, M.L. Ferrándiz, E. Aznar, F. Sancenón, M.J. Alcaraz, J.R. Murguía, M.D. Marcos, R. Martínez-Mañez, A.M. Costero, M. Orzáez, Targeting inflammasome by the inhibition of caspase-1 activity using capped mesoporous silica nanoparticles, *J. Control. Release*. 248 (2017) 60–70.
- [29] A. Ultimo, C. Giménez, P. Bartovsky, E. Aznar, F. Sancenón, M.D. Marcos, P. Amorós, A.R. Bernardo, R. Martínez-Mañez, A.M. Jiménez-Lara, J.R. Murguía, Targeting Innate Immunity with dsRNA-Conjugated Mesoporous Silica Nanoparticles Promotes Antitumor Effects on Breast Cancer Cells, *Chem. Eur. J.* 22 (2016) 1582–1586.
- [30] E. Aznar, C. Coll, M.D. Marcos, R. Martínez-Mañez, F. Sancenón, J. Soto, P. Amorós, J. Cano, E. Ruiz, Borate-Driven Gate-like Scaffolding Using Mesoporous Materials Functionalised with Saccharides, *Chem. Eur. J.* 15 (2009) 6877–6888.
- [31] E. Bringas, O. Koysuren, D. V Quach, M. Mahmoudi, E. Aznar, J.D. Roehling, M.D. Marcos, R. Martínez-Mañez, P. Stroeve, Triggered release in lipid bilayer-capped mesoporous silica nanoparticles containing SPION using an alternating

- magnetic field, *Chem. Commun.* 48 (2012) 5647–5649.
- [32] A. Agostini, L. Mondragón, A. Bernardos, R. Martínez-Máñez, M.D. Marcos, F. Sancenón, J. Soto, A. Costero, C. Manguan-García, R. Perona, M. Moreno-Torres, R. Aparicio-Sanchis, J.R. Murguía, Targeted Cargo Delivery in Senescent Cells Using Capped Mesoporous Silica Nanoparticles, *Angew. Chem. Int. Ed.* 51 (2012) 10556–10560.
- [33] C. de la Torre, I. Casanova, G. Acosta, C. Coll, M.J. Moreno, F. Albericio, E. Aznar, R. Mangues, M. Royo, F. Sancenón, R. Martínez-Máñez, Gated Mesoporous Silica Nanoparticles Using a Double-Role Circular Peptide for the Controlled and Target-Preferential Release of Doxorubicin in CXCR4-Expressing Lymphoma Cells, *Adv. Funct. Mater.* 25 (2015) 687–695.
- [34] L. Polo, N. Gómez-Cerezo, E. Aznar, J.-L. Vivancos, F. Sancenón, D. Arcos, M. Vallet-Regí, R. Martínez-Máñez, Molecular gates in mesoporous bioactive glasses for the treatment of bone tumors and infection, *Acta Biomater.* 50 (2017) 114–126.
- [35] C. Navarro, I. González-Álvarez, M. González-Álvarez, M. Manku, V. Merino, V.G. Casabó, M. Bermejo, Influence of polyunsaturated fatty acids on Cortisol transport through MDCK and MDCK-MDR1 cells as blood–brain barrier in vitro model, *Eur. J. Pharm. Sci.* 42 (2011) 290–299.
- [36] F. Torres-Molina, J.E. Peris, M.C. Garcia-Carbonell, J.C. Aristorena, L. Granero, J. Chesa-Jimenez, Use of rats chronically cannulated in the jugular vein and the duodenum in pharmacokinetic studies. Effect of ether anesthesia on absorption of amoxicillin, *Arzneimittelforschung* 46 (1996) 716–719.
- [37] G.P. Morris, P.L. Beck, M.S. Herridge, W.T. Depew, M.R. Szewczuk, J.L. Wallace, Hapten-induced model of chronic inflammation and ulceration in the rat colon, *Gastroenterology* 96 (1989) 795–803.
- [38] W.J. Sandborn, S.B. Hanauer, Systematic review: the pharmacokinetic profiles of oral mesalazine formulations and mesalazine pro-drugs used in the management of ulcerative colitis, *Aliment. Pharmacol. Ther.* 17 (2003) 29–42.
- [39] G. Hartmann, C. Bidlingmaier, B. Siegmund, S. Albrich, J. Schulze, K. Tschoep, A. Eigler, H.A. Lehr, S. Endres, Specific type IV phosphodiesterase inhibitor rolipram mitigates experimental colitis in mice, *J. Pharmacol. Exp. Ther.* 292 (2000) 22–30.
- [40] A. Lamprecht, N. Ubrich, H. Yamamoto, U. Schafer, H. Takeuchi, P. Maincent,

- Y. Kawashima, C.M. Lehr, Biodegradable nanoparticles for targeted drug delivery in treatment of inflammatory bowel disease, *J. Pharmacol. Exp. Ther.* 299 (2001) 775–781.
- [41] K. Mladenovska, R.S. Raicki, E.I. Janevik, T. Ristoski, M.J. Pavlova, Z. Kavrakovski, M.G. Dodov, K. Goracinova, Colon-specific delivery of 5-aminosalicylic acid from chitosan-Ca-alginate microparticles, *Int. J. Pharm.* 342 (2007) 124–136.
- [42] C. Mura, A. Nacher, V. Merino, M. Merino-Sanjuan, C. Carda, A. Ruiz, M. Manconi, G. Loy, A.M. Fadda, O. Diez-Sales, N-Succinyl-chitosan systems for 5-aminosalicylic acid colon delivery: in vivo study with TNBS-induced colitis model in rats, *Int. J. Pharm.* 416 (2011) 145–154.
- [43] J. Zhang, X. Li, J.M. Rosenholm, H. Gu, Synthesis and characterization of pore size-tunable magnetic mesoporous silica nanoparticles, *J. Colloid Interface Sci.* 361 (2011) 16–24.
- [44] C.T. Kresge, M.E. Leonowicz, W.J. Roth, J.C. Vartuli, J.S. Beck, Ordered mesoporous molecular sieves synthesized by a liquid-crystal template mechanism, *Nature.* 359 (1992) 710–712.
- [45] J. El Haskouri, S. Cabrera, M. Caldés, J. Alamo, A. Beltrán-Porter, M.D. Marcos, P. Amorós, D. Beltrán-Porter, Ordered mesoporous materials: Composition and topology control through chemistry, *Int. J. Inorg. Mater.* (2001) 1157–1163.
- [46] E.P. Barrett, L.G. Joyner, P.P. Halenda, The Determination of Pore Volume and Area Distributions in Porous Substances. I. Computations from Nitrogen Isotherms, *J. Am. Chem. Soc.* 73 (1951) 373–380.
- [47] S. Brunauer, P.H. Emmett, E. Teller, Adsorption of Gases in Multimolecular Layers, *J. Am. Chem. Soc.* 60 (1938) 309–319.
- [48] É. Pérez-Esteve, M. Ruiz-Rico, C. De La Torre, L.A. Villaescusa, F. Sancenón, M.D. Marcos, P. Amorós, R. Martínez-Mañez, J.M. Barat, Encapsulation of folic acid in different silica porous supports: A comparative study, *Food Chem.* 196 (2016) 66–75.
- [49] S.H. Lee, E. Moroz, B. Castagner, J.-C. Leroux, Activatable cell penetrating peptide-peptide nucleic acid conjugate via reduction of azobenzene PEG chains, *J. Am. Chem. Soc.* 136 (2014) 12868–12871.
- [50] Y.-Y. Yang, M. Grammel, A.S. Raghavan, G. Charron, H.C. Hang, Comparative analysis of cleavable azobenzene-based affinity tags for bioorthogonal chemical

- proteomics, *Chem. Biol.* 17 (2010) 1212–1222.
- [51] A.G. Oomen, C.J.M. Rompelberg, M.A. Bruil, C.J.G. Dobbe, D.P.K.H. Pereboom, A.J.A.M. Sips, Development of an in vitro digestion model for estimating the bioaccessibility of soil contaminants, *Arch. Environ. Contam. Toxicol.* 44 (2003) 281–287.
- [52] C.H.M. Versantvoort, A.G. Oomen, E. Van de Kamp, C.J.M. Rompelberg, A.J.A.M. Sips, Applicability of an in vitro digestion model in assessing the bioaccessibility of mycotoxins from food, *Food Chem. Toxicol.* 43 (2005) 31–40.
- [53] H. Tozaki, T. Fujita, J. Komoike, S.I. Kim, H. Terashima, S. Muranishi, S. Okabe, A. Yamamoto, Colon-specific delivery of budesonide with azopolymer-coated pellets: therapeutic effects of budesonide with a novel dosage form against 2,4,6-trinitrobenzenesulphonic acid-induced colitis in rats, *J. Pharm. Pharmacol.* 51 (1999) 257–261.
- [54] H. Tozaki, T. Odoriba, N. Okada, T. Fujita, A. Terabe, T. Suzuki, S. Okabe, S. Muranishi, A. Yamamoto, Chitosan capsules for colon-specific drug delivery: enhanced localization of 5-aminosalicylic acid in the large intestine accelerates healing of TNBS-induced colitis in rats, *J. Control. Release* 82 (2002) 51–61.
- [55] M. Naeem, J. Cao, M. Choi, W.S. Kim, H.R. Moon, B.L. Lee, M.-S. Kim, Y. Jung, J.-W. Yoo, Enhanced therapeutic efficacy of budesonide in experimental colitis with enzyme/pH dual-sensitive polymeric nanoparticles, *Int. J. Nanomedicine* 10 (2015) 4565–4580.